Shocklet structure of very high-β Earth bow shocks

A. A. Petrukovich[1] **and O. M. Chugunova**[1]

[1]Space Research Institute of Russian Academy of Sciences, Moscow, Russia

Key Points:

- 26 Earth bow shock crossings with extreme solar wind $\beta > 30$ are catalogued during 1995–2020.
- Many crossings have peculiar layout with many periodic (5–20 sec) shocklets.
- Shocklets are filled with partially thermalised plasma, bunched in one-second flow pulses coupled with strong magnetic variations.

Corresponding author: A.A. Petrukovich, a.petrukovich@cosmos.ru

Abstract

Observations of Earth's bow shock with very high $\beta \geq 10$ (ratio of thermal to magnetic pressure) are extremely rare. However, such shocks are supposed to be ubiquitous in astrophysical plasmas. We present statistics of several tens $\beta > 10$ shocks for MMS, Cluster and Geotail, 26 of which have $\beta > 30$. For the latter subset the most of crossings reveal very complex structure with quasi periodic shocklets, gradually thermalising the solar wind ion flow. One fortuitous MMS shock event allowed to study this phenomenon with unprecedented details. Each shocklet, in turn, consists of very high-amplitude magnetic oscillations with the period about 1 sec, coupled with the pulses of the plasma flow. These variations have wavelength about 150 km and are almost standing in the plasma rest frame, consistent with the expectation for Weibel mode. All together, the transition interval may last 5–10 min, but corresponds to a proton cyclotron scale in the solar wind, due to very low magnetic field and very slow shock motion.

Plain Language Summary

Collisionless shocks are very frequent and important objects in astrophysical plasmas. Earth's bow shock allow to study them in detail with in-situ experiments. However not all shock types are readily available in the solar wind. We present the detailed analysis of very rare shock with very low magnetic field.

1 Introduction

Earth's bow shock is the only readily accessible for in-situ measurements example of space collisionless shocks. In the rarefied magnetised plasmas a wide variety of shock types exists with quite differing structure (Kennel et al., 1985). The magnetic field vector is a key parameter in the Rankine-Hugoniout equations, governing the relation between upstream and downstream conditions. However, in the absence of collisions, specific kinetic mechanisms of field-particle interactions govern bulk flow slow-down and acceleration of some particles (Sagdeev, 1966; V. Krasnoselskikh et al., 2013). In the quasi-perpendicular shock geometry (when the angle between the shock normal and the upstream magnetic field is closer to 90^o) ions cannot escape upstream and a step-like shock transition forms with the overall width of several thousand km. In the quasi-parallel geometry (the angle is closer to 0^o) ions are capable to escape upstream along the magnetic field, a shock transition smears to the scales around several Earth radii, ions are efficiently accelerated locally, downstream flow becomes very structured (Scudder et al., 1986; Burgess et al., 2005; Turner et al., 2018; Plaschke et al., 2018).

Kinetic mechanisms evoke at a shock front low frequency (from one tenth to few Hz) and high-amplitude magnetic variations, actually dissipating ions. The specific unstable wavemode depends on magnetic geometry, β, Mach number, etc. In a supercritical quasi-perpendicular shock, the oblique whistler waves ($\sim$5 Hz) form the magnetic jump (V. V. Krasnoselskikh et al., 2002). In quasi-parallel shocks, series of substructures, known as SLAMS or shocklets, are formed, which gradually thermalise plasma flow (Lefebvre et al., 2009).

However, solar wind plasmas do not exhibit the whole range of parameters, defining the shock types. In particular, shocks in a weak magnetic field environment (high-β shocks) are common in interstellar and intergalaxy space (Markevitch & Vikhlinin, 2007; Donnert et al., 2018). β is a dimensionless parameter, the ratio of plasma thermal to magnetic energy density. Typical β in solar wind is around unity, shocks with $\beta > 10$ are rather rare, and only several dozens of cases with β closer to a hundred are potentially available.

Only very few examples of high-β events have been investigated. Formisano et al. (1975) presented three cases of OGO-5 spacecraft observations with β equal to 8, 170, 49, mentioning large magnetic field excursions. Winterhalter and Kivelson (1988) stated that shock appearance with high-amplitude magnetic variations is typical for the cases with higher β. Farris et al. (1992) investigated one shock with β equal to 18, checking the validity of Rankine-Hugoniot conditions and also mentioning high-amplitude magnetic variations.

In our previous investigation (Petrukovich et al., 2019) (hereafter cited as PCS19) we conducted a thorough analysis $\beta > 10$ occurrence in solar wind and of shocks in such conditions. A verified dataset of 22 shock crossings, observed by Cluster multispacecraft mission with the minimal spacecraft separation from several tens to couple hundred km, was presented. Intervals with $\beta > 10$ are related with the low speed, high density solar wind flow and very low interplanetary magnetic field 1–2 nT and are often quite transient. Discovered relatively compact large-scale structure of the observed shock transitions (about couple of minutes) is similar to that earlier reported for oblique and quasi-perpendicular shocks. It is distinctly different from the structure of quasi-parallel shocks, which are extended up to several Earth radii (Burgess et al., 2005). The apparent increased width of the magnetic jump (up to about 30 seconds) is mostly related with the slow shock motion and increased cyclotron radius. Observed magnetic variations are different from that for supercritical shocks with $\beta \sim 1$. Dominating magnetic variations in the shock transition have amplitudes much larger than the background field and frequency of ∼0.3–0.5 Hz (in some events — 1–2 Hz). The wave polarisation has no stable phase and is closer to linear, complicating determination of the wave propagation direction. The spatial scales (wavelengths) of variations are within several tens to couple hundred km.

In this publication we continue investigation of high β shocks with the substantial increase of statistics of verified crossings, including almost the full list for $\beta > 30$. This latter set is specially screened for any possible peculiarity of the shock structure. And, in fact, a novel type of shock profiles is found, rather typical for $\beta > 30$ and almost not observed in lower β events (10–30). It is in a sense, intermediate between quasi-parallel and quasi-perpendicular profiles. The crossing is quite compact (about ten min between undisturbed solar wind and magnetosheath), but consists of quasi periodic enhancements (shocklets), gradually thermalising the flow and merging in the downstream state. Using a fortuitous event, registered by MMS, we are able to trace ion dynamics down to the subsecond range, revealing stunning periodicities. We also discuss statistics of other observations.

2 Assembling the shock statistics

High-β shocks crossings are not frequent and usually clustered at the occasions of the specific solar wind with low bulk speed, high number density and low IMF (see PCS19 for the detailed solar wind statistics and details of the search procedure). We used 1-hour OMNI data set to automatically find hours with $\beta > 10$ and a spacecraft within 5 R_E from the model bow shock (Farris et al., 1991). All observations during 1995–2020 with Geotail, Interball, THEMIS, Cluster, MMS spacecraft are checked. For this initial lookout we take OMNI, ephemeris and spin-averaged magnetic field from CDAWeb archive. β values are precalculated in OMNI-2, assuming constant electron temperature (140000 K), He++ fraction (0.05) and He++ temperature (four times larger than proton temperature).

For each selected hour (in OMNI), the 5-hour window around it is reviewed visually. We pick up only crossings with the clear jumps in magnetic field and ion moments, as well as located within the stable high $\beta > 10$ intervals (here 1-min OMNI was used). Such a criterion may result in missing some quasi-parallel shocks, which have very smeared

profiles, but the expected proportion of such events should be rather small, assuming uniform distribution of IMF direction relative to shock normals.

This preliminary list contains several hundred candidate events. They, however, need further confirmation, regarding local upstream β value, data availability etc. We also excluded partial crossings, and crossings that occurred at a sharp β (mostly ion density) change. In PCS19 we selected and verified 22 Cluster project events for 2003–2012 with the relatively small separation (few tens or couple hundred km) between at least two spacecraft. This criterion was chosen in PCS19 to estimate the spatial scale of high-amplitude magnetic variations, forming the shock transition. Hereafter, for the sake of completeness, it is listed in Table S4 in Supplement.

In the current publication we add several new verified subsets. Table S2 contains 20 crossings of MMS spacecraft for 2017–2020, optimal to study plasma dynamics with high temporal resolution and to determine spatial scales. Several cases with actual $\beta <$ 10 were left in this dataset to facilitate any comparisons in future. Table S3 contains 20 crossings of Geotail spacecraft with $\beta > 10$. We also checked Interball and THEMIS crossings, but mostly they occurred with no high-resolution (16 Hz) magnetic field data, which are necessary to identify some important details of shock crossings (see PCS19 and below). Therefore, we do not provide separate tables for these spacecraft.

The main topic of this investigation, a collection of shocks with very high $\beta > 30$ is listed in Table S1 with 26 events for 1995–2020 years. The scope of Table S1 is wider, then just a subset of Tables S2,S3,S4. Geotail and MMS Tables S2 and S3 indeed have the almost full coverage (events were excluded only basing on quality requirements). The $\beta > 30$ events from Tables S2 and S3 are just copied to Table S1. Besides that, for Table S1 we additionally looked through THEMIS and Interball crossings, as well as through Cluster crossings, not covered by the Table S4 (which has the additional strongly restricting criterion on spacecraft separation distance). The threshold $\beta = 30$ as a characteristic of extreme cases was selected to keep the list substantial, but short enough, and is justified with further investigation.

Finally for the Table S1 we rechecked variability of upstream β. The main β variant, used in all tables, is the OMNI value, taken at 1-min point nearest to the shock crossing. Additionally we provide in Table S1 OMNI β and total magnetic field averaged within 12 min intervals, centred at the shock crossings. We also compute the local β estimate at some unperturbed solar wind interval, nearest to the shock. Since plasma measurements by MMS, Cluster, Geotail, Interball, THEMIS, are not exactly comparable with that of the interplanetary spacecraft, we use only local magnetic field for our estimate. We adjust OMNI β with the squared ratio of local upstream magnetic field and OMNI IMF. Since IMF is more variable, than the solar wind ion moments, and affects β strongly with a square law, such an approach looks quite reasonable.

Though three variants of β values (columns I,J,K in Table S1) are sometimes very different, there is no definite systematic change (e.g., overestimate in OMNI), except some extreme large OMNI $\beta > 100$ are actually smaller locally. It is quite reasonable, since extreme β appear, when IMF is occasionally very close to zero. Such dropouts could be relatively small structures, which may evolve between L1 point and a bow shock. The detailed discussion of OMNI β variability and reliability is in PCS19.

For analysis we used full-resolution Cluster FGM magnetic field (here with the sampling ~20 Hz) (Balogh et al., 2001) and HIA/CODIF ion data (sampling once in 4–12 s, depending on a parameter) (Rème et al., 2001) from Cluster Science Archive, Geotail MGF (Kokubun et al., 1994) (16 Hz) and LEP (Mukai et al., 1994) (12 sec) data from DARTS ISAS archive, Interball magnetic field (Nozdrachev et al., 1998) (16 Hz), Level 2 THEMIS FGM (16 Hz) and ESA (3 sec) (Angelopoulos, 2008; Auster et al., 2008; McFadden et al., 2008), MMS MGF (Russell et al., 2016) (128 Hz) and FPI (Pollock et al.,

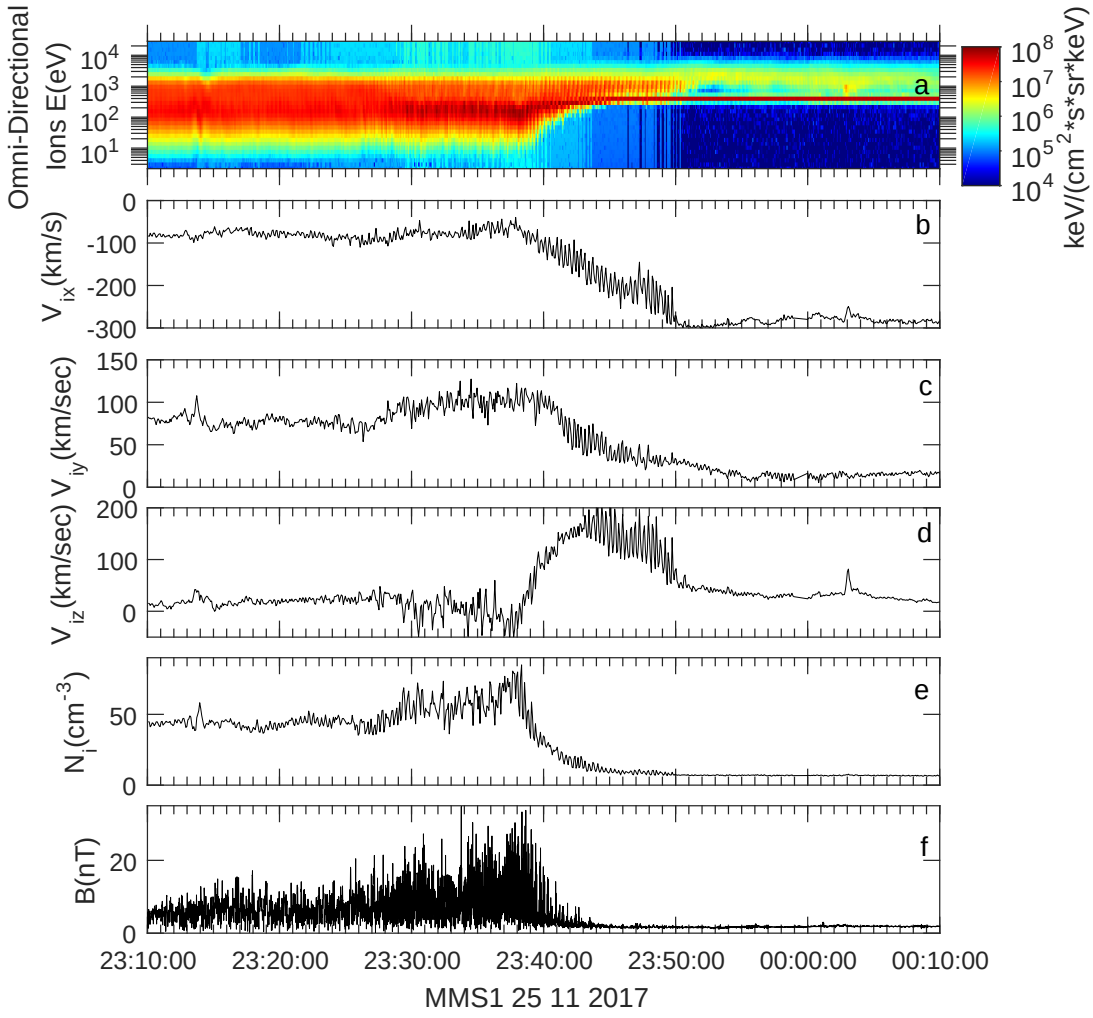

Figure 1. Overview of MMS crossing for event 25 November 2017. (a) ion omnidirectional spectrogram, (b-e) ion velocity and density, (f) magnetic field magnitude.

2016) (0.1 Hz in Burst mode) data from CDAWeb archive. All vectors in this paper are in GSE frame of reference. In the next section MMS1 data are used, if not explicitly mentioned otherwise.

3 Shock example

3.1 General structure

The shock crossing of interest occurred on 25 November 2017 around 23:40 UT. It is the only MMS event with the described phenomenon, but, fortunately, it is also a brightest example. The interval 23:10–00:10 UT covers the large-scale view (Figure 1). MMS Fast mode data are used in this figure. The shorter interval 23:35–23:45 UT of the Burst mode is in Figure 2.

MMS spacecraft are sunward and somewhat duskward from Earth with the spacecraft separation about 30 km. OMNI solar wind speed is small ∼335–340 km/s, density

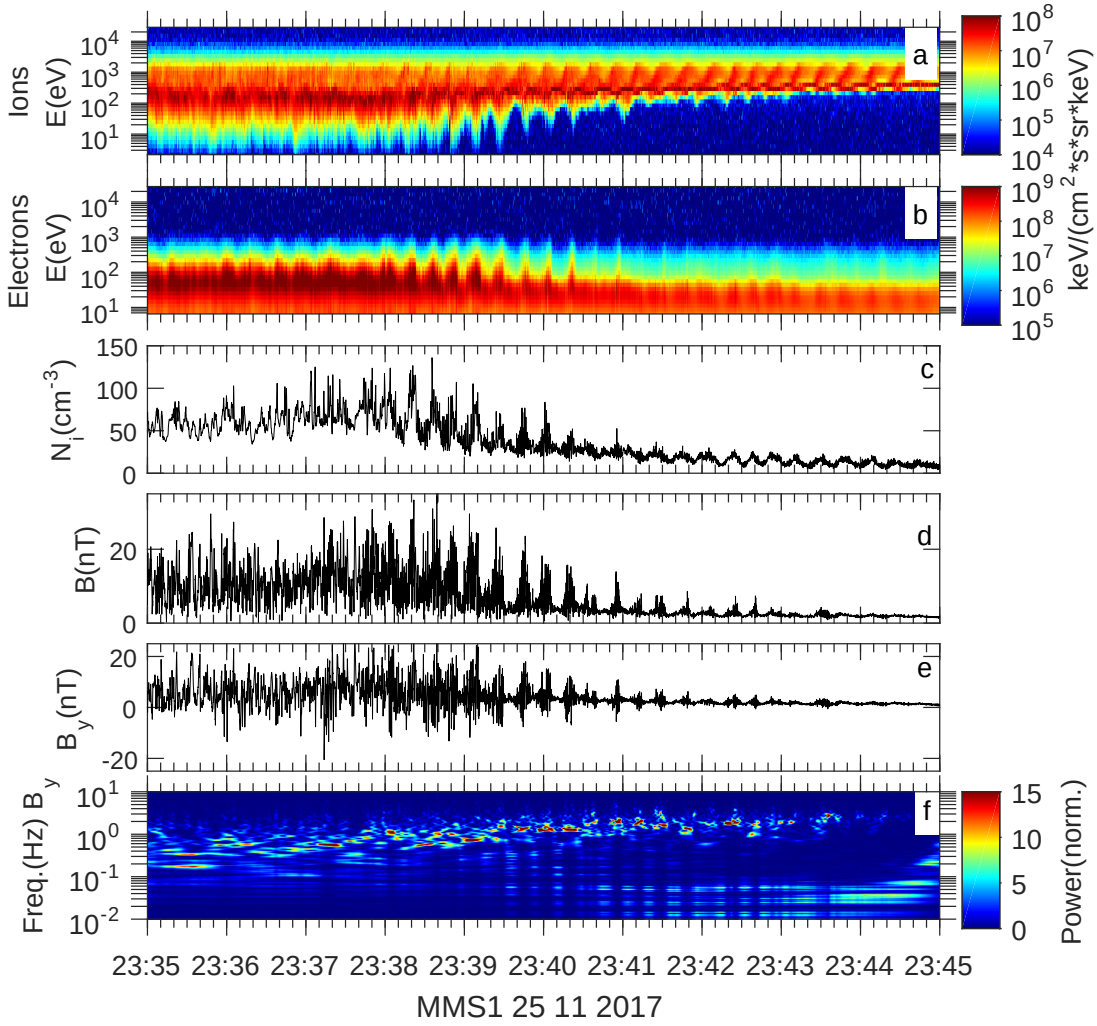

Figure 2. Overview of MMS crossing for event 25 November 2017, for the burst mode interval. (a) ion omnidirectional spectrogram, (b) electron omnidirectional spectrogram, (c) ion density, (d) magnetic field magnitude, (e) B_y magnetic field, (f) wavelet dynamic spectrum of magnetic field B_y.

is moderately high ∼9 cm^{-3} (all characteristics are in Table S1 or S2). According to 1-min OMNI data, IMF magnitude is 0.9 nT, resulting in very high $\beta = 66$ and Alfvén Mach number ∼60. Magnetosonic Mach number is 7. These values are stable on a scale of one hour. Local (measured by MMS) solar wind ion bulk speed is somewhat less than 300 km/s, but one should note, that FPI is not a dedicated solar wind instrument. Upstream electron bulk velocity (not shown here) is closer to the OMNI value. Local IMF (e.g., at 23:50 UT) is about twice larger than that in OMNI, resulting in local upstream β only about 16. However, this crossing has substantial amount of reflected ions, which may lead to some increase of magnetic field in the foreshock.

The model shock normal (Farris et al., 1991) is almost sunward, and the resulting θ_{Bn} angle is 68^o for OMNI magnetic field and 59^o for local magnetic field, so the shock geometry is determined reliably and is close to quasi perpendicular. The compression ratios of magnetic field and ion density are close to four, typical for supercritical shocks.

However, for about of couple of minutes 2335–2340 UT the ion density is up to 2–3 time higher than the final downstream value. We place the main shock transition at 23:38–23:39 UT, when magnetic field and ion density stably reach the downstream level.

The plasma flow completely relaxes well behind the shock front, approximately at 2325 UT (Figure 1), when oscillations in ion density and bulk velocity subside. The final downstream bulk velocity is ≈–80, 80, 10 km/s both for ions and electrons. The magnetosheath plasma flow here is close to stagnation, because of proximity to the magnetopause.

Substantial suprathermal ion population is also present upstream. The transition zone can be identified qualitatively as 23:38–23:50 UT, basing on the substantial presence of reflected ions, affecting the ion bulk velocity components. Taking into account very low magnetic field, as well as, very low (expected, see Sec. 5) speed of the shock motion, the spatial length of this 12-min interval is actually of the order of a proton cyclotron radius in solar wind.

The main peculiar feature of this shock transition is rich variability (Fig.2). The dominating upstream signature are the periodic enhancements of ion density and magnetic field with the stable frequency 0.05–0.06 Hz (period slightly smaller than 20 seconds, Fig. 2f). We name such enhancements as shocklets, similar to a quasi-parallel shock. Amplitudes of shock lets grow towards downstream, and finally these enhancements merge in a continuous downstream state. Electron spectrogram (Fig. 2b) reveals periodic energy and density increases, following magnetic field changes. Ion spectrogram (Fig. 2a) reveals substantial changes of ion populations also inside shocklets, which are described in detail in the next subsection. Each such shocklet, being formally located upstream, actually contributes to thermalisation of the ion flow. Another characteristic oscillation of magnetic field and ion density is embedded inside shocklets. It has the frequency about 0.5–2 Hz, decreasing towards downstream (Fig. 2f).

In the following we concentrate on the interval 23:38–23:45 UT with the most pronounced periodic structures and select three characteristic shocklets. However, it is almost impossible to describe all observed details in a single investigation. In particular, we leave the reconstruction of the full 3D ion kinetics to the future studies.

3.2 Shocklets

We choose three intervals, each including one "shocklet": #1 in the distant upstream with 23:43:23–23:43:38 UT , #2 in more mature foreshock 23:40:14–23:40:26 UT, and #3 almost at a shock front, but still upstream, 23:39:00–23:39:12 UT (Figures 3–8).

The upstream shocklet #1 occurs on the background of almost undisturbed solar wind and IMF, mostly as an enhancement of the net magnetic field magnitude from 2 to 3 nT and of ion density from 10 to 15 cm^{-3} (Fig.3).All specific shocklet signatures, described here, are more developed and evident in shocklets #2 and #3). In a more detailed view, the magnetic magnitude enhancement consists of the magnetic variations with the amplitudes of the order of the background IMF. In the ion overview data (energy spectrograms, Fig. 3a, Fig. 4), this magnetic and density enhancement is accompanied by a slight slowdown and rotation of the solar wind flow towards the future downstream state, as well as by the appearance of the Earth-streaming high-energy component (in $-X$ spectrogram of Fig. 4).

The reflected ions in $+X$ and $+Z$ are present not only in shock lets, but also throughout the foreshock. $+X$ flow is more intense towards the shock-ward edge of the shocklet, but their energy increases towards upstream.

There is also a stable ion density periodicity $\leq$1 sec (Fig. 3b). It likely corresponds to the known caveat of MMS measurements in the solar wind: the narrow solar wind ion

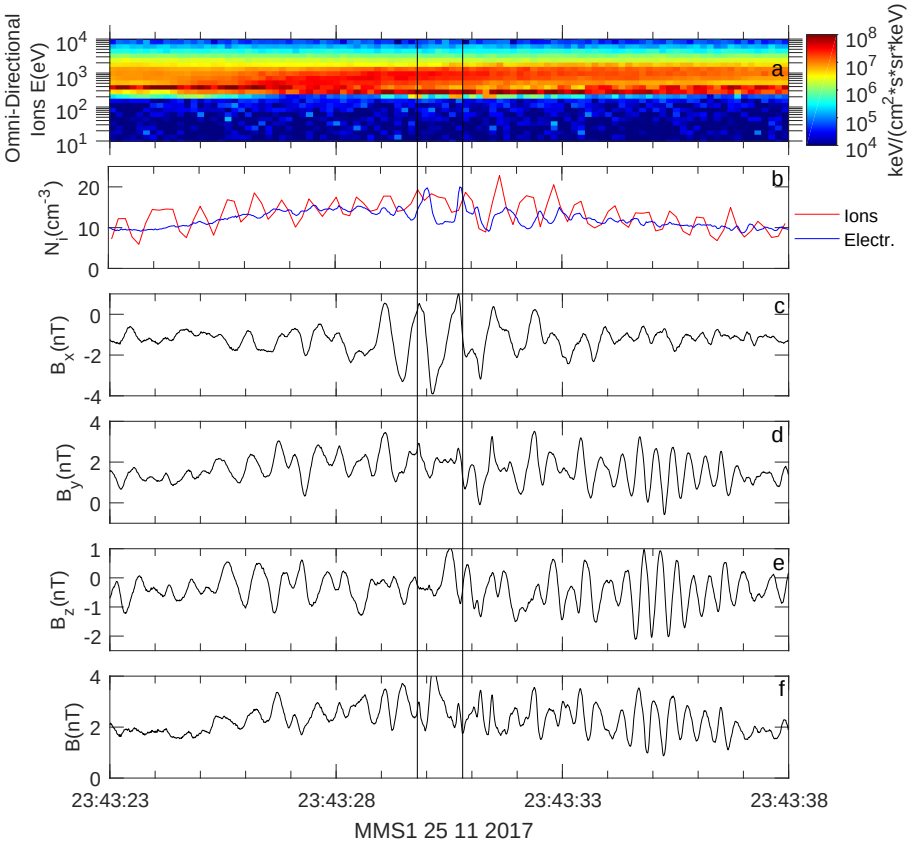

Figure 3. Overview of shocklet #1. (a) ion omnidirectional spectrogram, (b) ion and electron density, (c-f) magnetic field vector and magnitude. Vertical lines denote two plasma density peaks.

beam periodically falls in between the FPI sensors. The 20-sec spacecraft period and 32 FPI azimuthal sectors result in a 20/32=0.65 s period, close to the observed one. Simultaneous electron density data confirm only two substantial density spikes (23:43:30, 23:43:31), which coincide with the maxima in B_x.

There are two clear wave packets. The first one at 23:43:34–23:43:37 UT is mostly in B_y and B_z components and with frequency 2.75 Hz. Its main wave characteristics are in Table 1. The temporal delays between MMS spacecraft are of the order of 0.1 sec, allowing reliable multipoint analysis (not shown here in detail). It is an elliptically polarised wave with the clear minimum variance direction, just 10^o away from the timing normal. The variance matrix was built using all four satellites to improve statistical accuracy. The Doppler shift in frequency is approximately equal to the observed frequency, suggesting the almost standing wave in the plasma rest frame. However, the timing velocity vector is not parallel to the nominal bulk flow velocity.

The second wave packet at 23:43:28–23:43:33 UT is mostly in B_x, has the linear polarisation (Table 1) and lower frequency. The maximum variance vector is orthogonal (within 10^o) to local magnetic field and the timing normal. The propagation direction (timing normal) is pointed closer to the final direction the downstream flow. As in the previous case, the Doppler shift is of the order of the observed frequency.

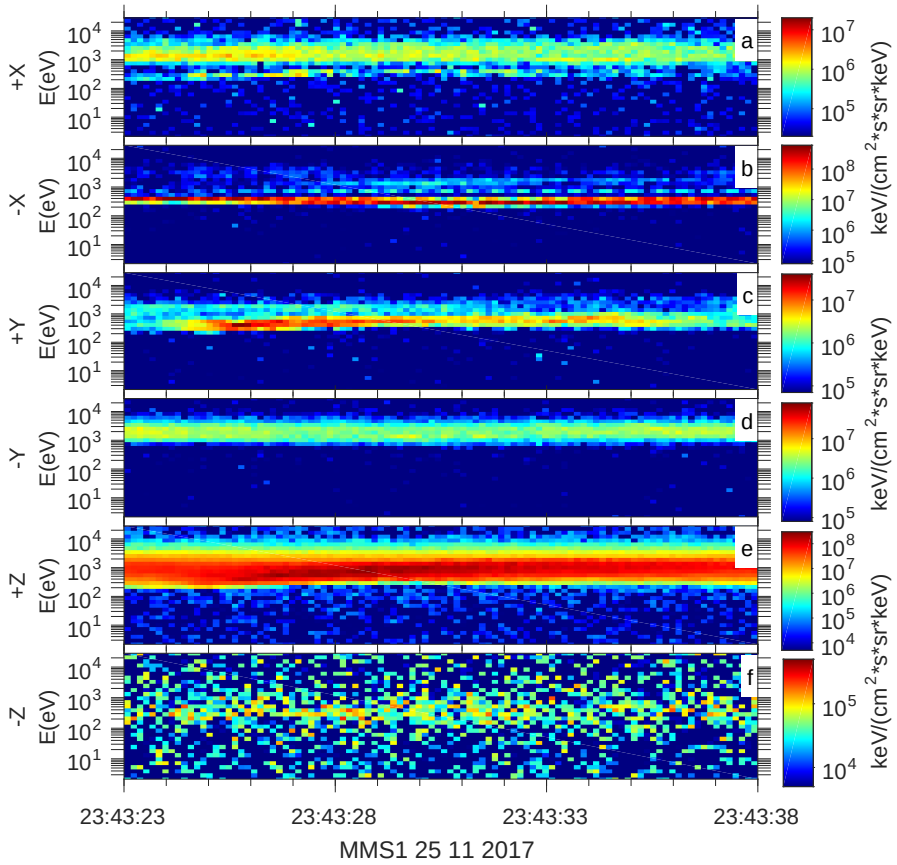

Figure 4. Ion spectrograms for six directions for shocklet #1.

The second sample shocklet (23:40:14–23:40:26 UT) occurs already in a substantially decelerated solar wind flow with the increased ion density (20–30 cm^{-3}) and magnetic field (3–5 nT) (Figure 5).

The magnetic field magnitude temporary enhancements are up to 10–15 nT, mostly in B_y and B_z components. Both ion and electron density peak up to 50 cm^{-3}. The properties of the clear magnetic wave packet 23:40:15–23:40:21.5 UT with linear polarisation are listed in Table 2 and are similar to that of the linearly polarised packet in the shocklet #1 (23:43:28–23:43:33 UT), as concerns frequency, velocity, maxvar direction, wavelength and Doppler shift. The peaks in magnetic field magnitude correspond to the extrema of components. Peaks in ion and electron density often correspond to (almost) maxima of B_x, but this feature is not confirmed on statistics.

The solar wind flow before and after Shocklet #2 is already substantially decelerated and is further thermalised within the shocklet (Fig. 6). There is also significant amount of high energy reflected ions. Sporadically low energy ions around 100 eV appear. The large density peaks correspond to clear enhancements of the magnetosheath-like ion flow ($\sim$(−160, 90, 50) km/s). The intervals between density peaks are almost void of the magnetosheath-type flow, contain less low energy and more high energy ions, including downstream directed (–X) 1000–2000 eV ions (23:40:15–23:40:18 UT). This small-scale bunching of the shocklet flow is barely visible in shocklet #1, is evident here, and is much more prominent in shocklet #3.

Table 1. Wave analysis data for shocklet #1.

Parameter	23:43:34–23:43:37 UT	23:43:28–23:43:33 UT
magnetic field, nT	–1.18, 1.42, –0.36	–1.21, 1.84, –0.38
ion bulk flow, km/s	–220, 55, 120	–180, 60, 150
peak frequency, Hz	2.75	1.2
eigenvalues	0.068 0.47 0.57	0.26 0.34 1.67
min(max) var vector	0.997, –0.050, 0.055	–0.87, –,0.46, –0.21
spacecraft delays vs MMS1, s	0.078, 0.039, –0.047	0.117, 0.117, 0.094
multipoint timing normal	0.992, –0.0404, –0.119	0.603, –0.760, –0.243
timing velocity, km/s	200.4	196
wavelength, km	72	163
Doppler shift, Hz	∼3	∼1.3
θ_{kB}	$\sim 40^o$	$\sim 35^o$

Table 2. Wave analysis data for shocklets 2 and 3.

Parameter	shocklet 2	shocklet 3
magnetic field, nT	–0.93, 3.63, –0.82	–1.67, 4.06, –1.17
ion bulk flow, km/s	–150, 90, 100	–100, 110, 70
peak observed frequency, Hz	1.25	0.8
eigenvalues	4.72, 5.78, 46.2	16.47, 19.49, 117.72
max var vector	0.8132, 0.5768, 0.0777	0.86, 0.47, 0.17
spacecraft delays vs MMS1, s	0.133, 0.133, 0.109	0.164, 0.171, 0.148
multipoint timing normal	0.591, –0.774, –0.230	0.539, –0.801, –0.262
timing velocity, km/s	173	139
wavelength, km	138	173
Doppler shift, Hz	∼1.3	∼0.9
θ_{kB}	$\sim 35^o$	$\sim 35^o$

The third sample shocklet (23:39:00–23:39:12 UT, contains almost magnetosheath type plasma (Fig. 7,8), but still is attributed to foreshock, since it is enveloped in the less thermalised solar wind flow. It also contains a typical magnetic wave packet at 23:39:00–23:39:09 UT. The magnetic field oscillations (5–30 nT) are mostly in B_x and B_y components. The properties of the packet are listed in Table 2 and are similar to that in shocklet #2, but the frequency is somewhat lower and the wavelength longer.

At least six clear ion density bursts, of the order of 1-sec duration and amplitudes up to 100 cm^{-3}, are coupled with magnetic variations. The density variations are almost identical in electron and ion data and the delays between the spacecraft are almost the same for magnetic field and density (see Figure 9 for a detailed plot). It should be noted, however, that while the magnetic field sampling 128 Hz is sufficient to measure delays of the order of 0.15 s reliably, the density sampling is marginally sufficient only to confirm delays equal to one sampling interval. Thus, it is not possible to make an independent timing of density peaks with the accuracy comparable with that for magnetic field time profiles. Also, there is no any clear correlation between density peaks and magnetic field magnitude and direction.

Ion spectrograms of shocklet #3 are similar to that of shocklet #2, but contain more thermalised plasma. The down-streaming hot ions are enhanced during the shocklet. The one-second flow periodicity is very well developed here. For example, during the ion den-

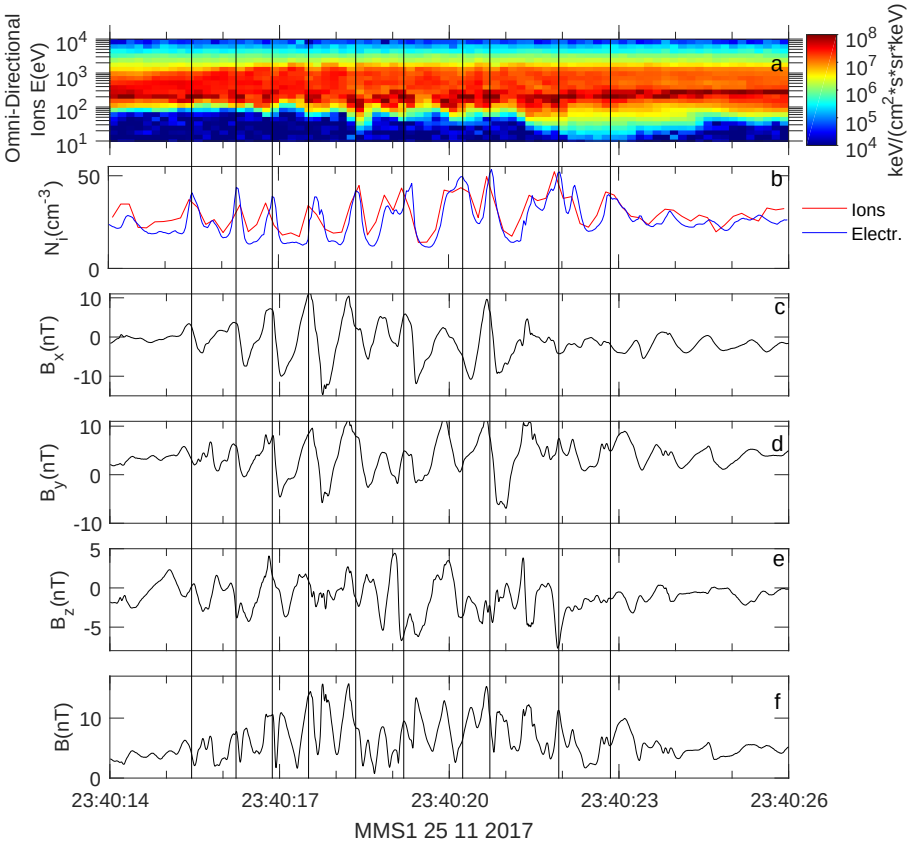

Figure 5. Overview of shocklet #2. (a) ion omnidirectional spectrogram, (b) ion and electron density, (c-f) magnetic field vector and magnitude. Vertical lines denote two plasma density peaks.

sity burst (23:39:06.120–23:39:06.870 UT) the ion flow has clear magnetosheath like direction ∼(–124, 95, 10) km/s, but still is different from the finally relaxed state ∼(–80, 80, 10) km/s. In the "gap" interval 23:39:07.020–23:39:07.470 UT there is much less magnetosheath-like flow and much more other ion populations, including upstreaming cold ions (100 eV) and downstreaming hot ions (1000 eV).

4 Other examples

The review of very high β crossings in Table S1 reveals that a quasi-periodic structure in the foreshock is present in 14 out of 26 cases. Column #2 contains a heuristic estimate of the quality of shocklets. Marks 2-3 are given, when a structure has a clear appearance, is filled with 1-Hz magnetic oscillations, but has some significant visual deficiencies, such as unequal spacing or small number of shocklets (but not less than 3). Marks 4-5 are given for very good examples. The shocklet period is in the range 5–20 s, and is provided in column 2 as, e.g., 'p15'.

Other 12 cases are considered with 'no shocklets'. Mark 1 is given for two events, when only slight increases of magnetic field are observed, with no internal magnetic oscillations, but accompanied with the slight deceleration of solar wind. In our main example, such enhancements are located in the upstream-most part 23:44–23:45 UT (Fig. 2). It is possible to identify such type mostly in the MMS cases, which have high cadence

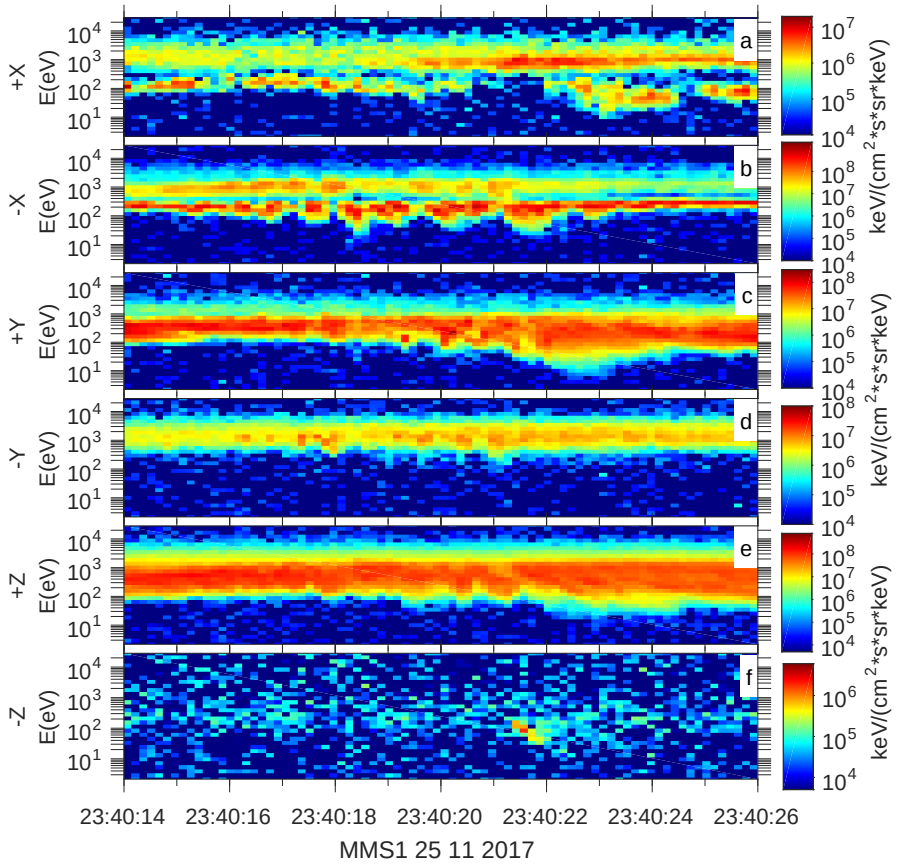

Figure 6. Ion spectrograms for six directions for shocklet #2.

ion measurements. Otherwise, it is difficult to interpret reliably magnetic variations. Finally, mark 0 denotes complete visual absence of the effect.

An initial attempt to determine statistically origins of these shocklet events failed. There is no substantial difference in β, solar wind parameters and IMF between shocklet and non-shocklet crossings. Moreover, in some Cluster examples (see below) the crossings by different spacecraft may exhibit almost simultaneously absence and presence of shocklets.

The criterion of 'very high-β' as $\beta > 30$ was selected initially just to compile some reasonable statistics of unique shocks. Later we recheck almost all available events with $\beta > 10-30$, to determine how important is indeed this specific β threshold for observation of periodic shocklets. Only one series of three shocks with shocklets was found additionally (Geotail, 1996 Nov 07, 10–17 UT) with OMNI $\beta = 11-17$. However, the local β was higher (15–43). It is marked in Table S3. Additionally four more events with very weak signatures (denoted as '1' in Table S2) were found in MMS data (marked in Table S2).

It should be mentioned that it is essential to have at least 16-Hz sampling of magnetic field to discover the event reliably in magnetic variations and about 1 Hz sampling of plasma moments to confirm plasma deceleration. To reveal in detail the internal structure of shocklets, one needs full MMS resolution of 128 Hz for magnetic field and 10 Hz for plasma.

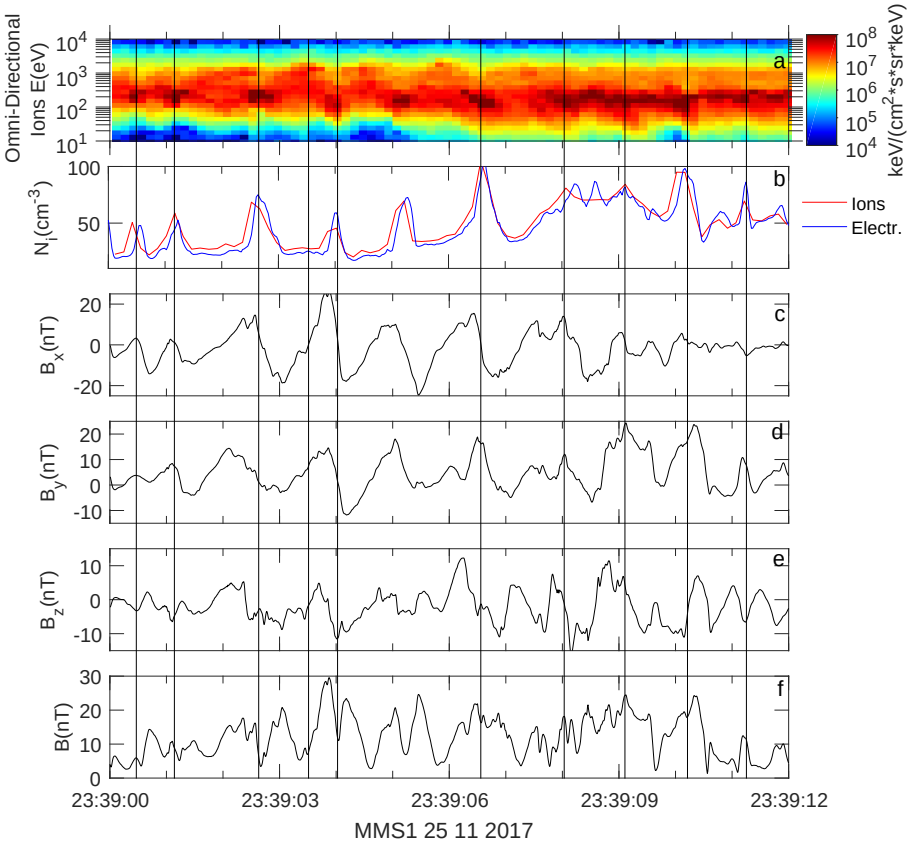

Figure 7. Overview of shocklet #3. (a) ion omnidirectional spectrogram, (b) ion and electron density, (c-f) magnetic field vector and magnitude. Vertical lines denote two plasma density peaks.

MMS spacecraft separation of several tens km allows to reveal the small-scale structure of shocklets (100–200 km), but the foreshock structure as a whole remains uncertain. Variety of the Cluster crossings potentially allows to use the larger spacecraft separations to visualize the large-scale structure. During late Cluster years only the distance between C3 and C4 was controlled, while the whole tetrahedron had the scale of several thousand km.

For two Cluster multispacecraft events with quasi-periodic structure (2007 Feb 05 and 2007 Mar 21) we determine the shock speed along the normal, which is very low (7.2 and 3.5 km/s respectively). Such low speeds were also found in PCS19 and are rather common for low speed solar wind (Kruparova et al., 2019) However, the distance between C3 and C4 equal to 400–600 km turned out to be too large for these particular events (Fig. 10 for 2007 Feb 05). The observed 1.5 min difference between crossings of C3 and C4 corresponds to 600 km separation, but C3 foreshock contains only weak signatures of shocklets, while C4 foreshock has many. Spacecraft C1 and C2, being several thousand km away (separations are in Table S1), observed also very differing profiles.

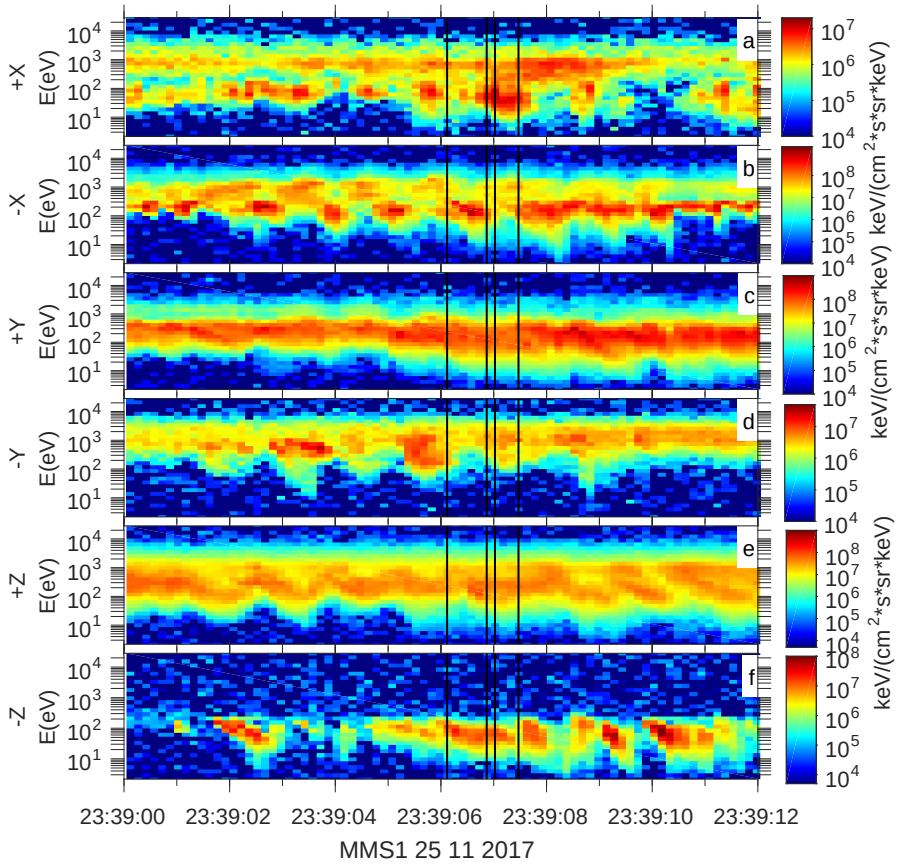

Figure 8. Ion spectrograms for six directions for shocklet #3. Vertical lines denote one plasma flow pulse interval at 23:39:06 UT and one interval between the pulses 23:39:07 UT (see text for details).

5 Discussion

5.1 General shock properties

Understanding the spatial structure of this new type of shock front with shocklets is of primary interest. Though MMS allows to reveal the scales about 10-s of km, unfortunately, the large-scale structure remains not fully clear. The Cluster project data only confirm strong differences on the scale of minutes and many hundred km.

First of all, one needs to keep in mind specifics of high β shocks related with the very low speed of proper shock motion (below 5–10 km/s) and the large kinetic scale due to the low magnetic field. Though our MMS case does not allow to determine the shock speed, assuming ∼5 km/s, one can get an estimate of 1500 km for a 5 min of observation. Therefore the reasonable foreshock length up to the most upstream shocklet is 1000–4000 km, of the order of proton gyroradius in low IMF.

The second important issue is remarkable stability of the shocklet periodicity. Their duration remains constant, and amplitude most often steadily grows, while one is approaching the shock front.

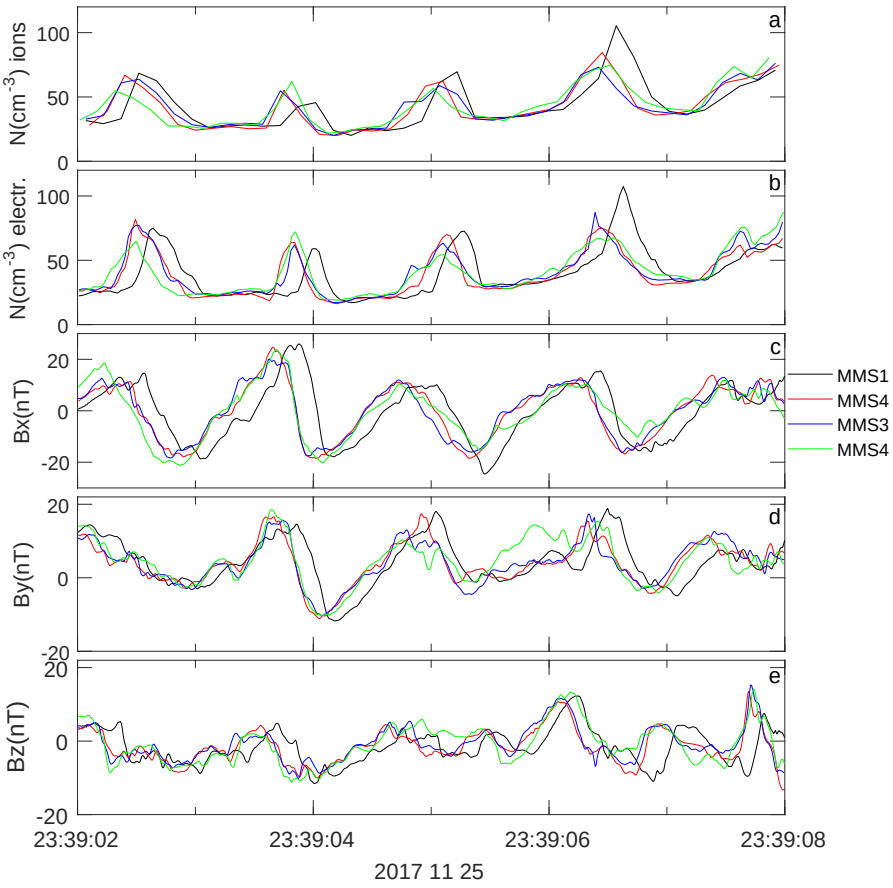

Figure 9. Multispacecraft time profiles of ion and electron density and magnetic field for the interval of the largest fluctuations in shocklet #3.

The frequency of the large-amplitude magnetic oscillations is steadily decreasing (from 3 to 0.5 Hz, Figure 2f), while the wavelength is increasing towards the shock front. However, the geometry of the wave packets is very stable and the most of the observed frequency is due to Doppler shift. These local structures are moving with ∼100 km/s. Therefore the 1-Hz density peaks and magnetic field maxima have the spatial scale of the order of 100–150 km along the local flow. The full wave packet in one shocklet (10 sec) likely has the length about 1000 km.

In the third place, this dynamic structure with shocklets is likely appearing on the background of a standard high-β shock (see PCS19 for examples and Fig. 10 with almost absent shocklets at Cluster 3 location).

Basing on these considerations one can suggest the following variants of the foreshock structure. The 'stationary' variant assumes, that shocklets are actually azimuthally-moving undulations on a shock front. In the maxima of undulations the shock transition is strongly smeared in the upstream direction. The gaps between shocklets are then 'valleys' between undulations. This scenario explains strict periodicity, but lacks understanding, why the shock transition is suddenly smearing so strongly and uniformly in many undulations to explain the ordering of shocklet amplitudes.

Alternatively, a shocklet might be born upstream as an 'island', if certain conditions are met with e.g., properties of the reflected ions. A shocklet gradually grows and

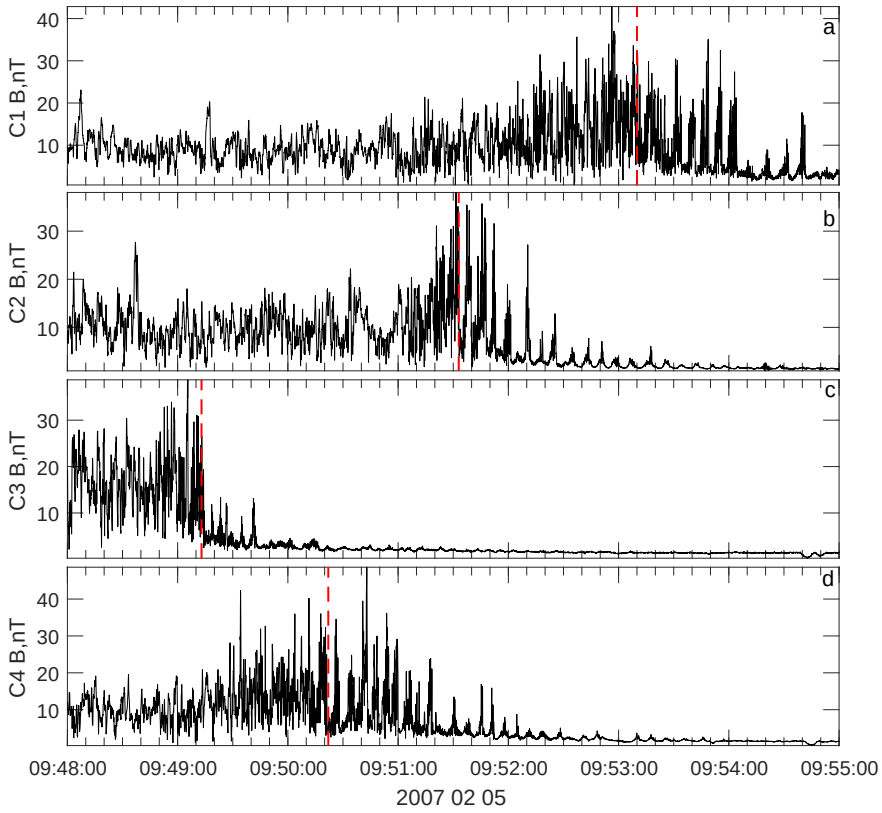

Figure 10. Magnitude of magnetic field for four Cluster spacecraft for the 2007 Feb 05 crossing. Vertical lines denote the presumed shock front positions.

deflects the solar wind flow. The growing magnetic variations break the solar wind flow in 1-s pulses, which become more prominent closer to a shock front. Simultaneously a shocklet is convected azimuthally and downstream with this flow. Then the lifespan of a shocklet of the order of 10 s and 1000 km, is enough to develop, propagate and merge with the shock front. In this scenario it is easy to explain amplitudes of shocklets, but difficult to explain the strict periodicity along the spacecraft trajectory.

The local plasma conditions, facilitating growth of shocklets and controlling their duration, remain unknown for now. One can, for example, underline downstreaming hot ions, registered within the shocklets, as possible candidates.

A final reply to this problem will require the detailed analysis of the 3d ion kinetics both in experiment and modeling. The multispacecraft mission will need a separation of the order of couple hundred km to observe the foreshock structure.

5.2 Magnetic variation properties

The properties of the dominating magnetic oscillations in the 2017-Nov-25 MMS case are consistent with that previously found in PCS19. Additionally, MMS mission allows full 3d linear reconstruction, rather then two-point estimates of the spatial characteristics. The wavelength is of the order of 150 km, observed frequency is about 1 Hz, polarisation is linear, the vector of maximal variation is stably orthogonal to the background magnetic field. The dominating frequency is decreasing towards downstream to

below 0.5 Hz also in consistency with PCS19 (in that examples oscillations were present only at and behind the shock front). The propagation direction is also orthogonal to the background magnetic field and is about 20^o away from the local bulk flow. The latter angle slightly depends on the definition of the bulk flow (an average during the shocklet or a value during the density peak), but, in any case, it is small. The Doppler shift is almost equal to the observed frequency, thus the magnetic wave is almost standing in the plasma rest frame, having the frequency not more than 10–20% of the observed one.

The observed wave properties are quite stable for the three studied wave packets (except the upstream-most elliptically polarized wave, which is set aside here). The coplanarity conjecture (Hubert et al., 1998) for compressive waves (the vectors of magnetic field, wavevector and maximum variation are coplanar) is likely invalid. Other interpretation variants are discussed in PCS19.

The described properties are consistent with the alternative hypothesis of Weibel mode, frequently suggested for high-β plasma and similar to drift mirror mode. With no seed magnetic field the Weibel mode has only imaginary frequency, that is, magnetic field variations are growing faster, than propagate. For a finite magnetic field, Pokhotelov and Balikhin (2012) suggested that the Weibel mode grows as a mix of two opposite circular polarisations, and has small real frequency. A more detailed analysis of additional plasma parameters such as electric field and electron distribution may help in the future identification of the wave mode. Another potentially interesting issue for the future study, is nonlinear coupling of these variations with the ion flow bursts, which helps to decelerate solar wind flow in the foreshock (Urbář et al., 2019).

6 Conclusions

The indepth study of very high β shocks ($\beta > 30$) revealed the novel type of shock structure, consisting of shocklets — 5–20 s enhancements of magnetic variations, gradually heating and deflecting the solar wind flow. The shock, however is quasi-perpendicular or oblique and the whole shock transition remains comparable with the proton gyroscale.

It is also interesting to note, that besides the high-resolution particle measurements, the slow shock motion (∼5 km/s) and large kinetic scale (due to low magnetic field) are also critical to reveal the proton dynamics within these shocklets. With more ordinary β and more typical faster shock motion (Kruparova et al., 2019) even MMS high measurement cadence would be likely insufficient.

Acknowledgments

The data analysis was supported with Russian Science Fund project 19-12-00313. We are thankful for the public project archives: Cluster Science Archive (https://csa.esac.esa.int/csaweb/), DARTS (http://darts.isas.jaxa.jp/), CDAWeb (https://cdaweb.gsfc.nasa.gov/) and OMNI (https://omniweb.gsfc.nasa.gov/) for availability of spacecraft data. High-resolution magnetic field data for one Interball-Tail spacecraft crossing is included as electronic supplement and will be uploaded to public repository after acceptance.

References

Angelopoulos, V. (2008, December). The THEMIS Mission. *Space Science Reviews*, *141*(1-4), 5-34. doi: 10.1007/s11214-008-9336-1

Auster, H. U., Glassmeier, K. H., Magnes, W., Aydogar, O., Baumjohann, W., Constantinescu, D., ... Wiedemann, M. (2008, December). The THEMIS Fluxgate Magnetometer. *Space Science Reviews*, *141*(1-4), 235-264. doi: 10.1007/s11214-008-9365-9

Balogh, A., Carr, C. M., Acuña, M. H., Dunlop, M. W., Beek, T. J., Brown, P.,

... Schwingenschuh, K. (2001, October). The Cluster Magnetic Field Investigation: overview of in-flight performance and initial results. *Annales Geophysicae*, *19*, 1207-1217. doi: 10.5194/angeo-19-1207-2001

Burgess, D., Lucek, E. A., Scholer, M., Bale, S. D., Balikhin, M. A., Balogh, A., ... Walker, S. N. (2005, June). Quasi-parallel Shock Structure and Processes. *Space Science Reviews*, *118*, 205-222. doi: 10.1007/s11214-005-3832-3

Donnert, J., Vazza, F., Brüggen, M., & ZuHone, J. (2018, December). Magnetic Field Amplification in Galaxy Clusters and Its Simulation. *Space Science Reviews*, *214*, 122. doi: 10.1007/s11214-018-0556-8

Farris, M. H., Petrinec, S. M., & Russell, C. T. (1991, October). The thickness of the magnetosheath: Constraints on the polytropic index. *Geophysical Research Letters*, *18*, 1821-1824. doi: 10.1029/91GL02090

Farris, M. H., Russell, C. T., Thomsen, M. F., & Gosling, J. T. (1992, December). ISEE 1 and 2 observations of the high beta shock. *Journal of Geophysical Research*, *97*, 19121-19127. doi: 10.1029/92JA01976

Formisano, V., Russell, C. T., Means, J. D., Greenstadt, E. W., Scarf, F. L., & Neugebauer, M. (1975, June). Collisionless shock waves in space: A very high β structure. *Journal of Geophysical Research*, *80*, 2013. doi: 10.1029/JA080i016p02013

Hubert, D., Lacombe, C., Harvey, C. C., Moncuquet, M., Russell, C. T., & Thomsen, M. F. (1998, November). Nature, properties, and origin of low-frequency waves from an oblique shock to the inner magnetosheath. *Journal of Geophysical Research*, *103*, 26783-26798. doi: 10.1029/98JA01011

Kennel, C. F., Edmiston, J. P., & Hada, T. (1985, January). A quarter century of collisionless shock research. *Washington DC American Geophysical Union Geophysical Monograph Series*, *34*, 1-36. doi: 10.1029/GM034p0001

Kokubun, S., Yamamoto, T., Acuña, M. H., Hayashi, K., Shiokawa, K., & Kawano, H. (1994, January). The GEOTAIL Magnetic Field Experiment. *Journal of Geomagnetism and Geoelectricity*, *46*(1), 7-21. doi: 10.5636/jgg.46.7

Krasnoselskikh, V., Balikhin, M., Walker, S. N., Schwartz, S., Sundkvist, D., Lobzin, V., ... Comisel, H. (2013, October). The Dynamic Quasiperpendicular Shock: Cluster Discoveries. *Space Science Reviews*, *178*, 535-598. doi: 10.1007/s11214-013-9972-y

Krasnoselskikh, V. V., Lembège, B., Savoini, P., & Lobzin, V. V. (2002, April). Nonstationarity of strong collisionless quasiperpendicular shocks: Theory and full particle numerical simulations. *Physics of Plasmas*, *9*, 1192-1209. doi: 10.1063/1.1457465

Kruparova, O., Krupar, V., Å afránková, J., Němeček, Z., Maksimovic, M., Santolik, O., ... Merka, J. (2019, March). Statistical Survey of the Terrestrial Bow Shock Observed by the Cluster Spacecraft. *Journal of Geophysical Research (Space Physics)*, *124*(3), 1539-1547. doi: 10.1029/2018JA026272

Lefebvre, B., Seki, Y., Schwartz, S. J., Mazelle, C., & Lucek, E. A. (2009, November). Reformation of an oblique shock observed by Cluster. *Journal of Geophysical Research (Space Physics)*, *114*, A11107. doi: 10.1029/2009JA014268

Markevitch, M., & Vikhlinin, A. (2007, May). Shocks and cold fronts in galaxy clusters. *Physics Reports*, *443*, 1-53. doi: 10.1016/j.physrep.2007.01.001

McFadden, J. P., Carlson, C. W., Larson, D., Ludlam, M., Abiad, R., Elliott, B., ... Angelopoulos, V. (2008, December). The THEMIS ESA Plasma Instrument and In-flight Calibration. *Space Science Reviews*, *141*(1-4), 277-302. doi: 10.1007/s11214-008-9440-2

Mukai, T., Machida, S., Saito, Y., Hirahara, M., Terasawa, T., Kaya, N., ... Nishida, A. (1994, January). The Low Energy Particle (LEP) Experlment onboard the GEOTAIL Satellite. *Journal of Geomagnetism and Geoelectricity*, *46*(8), 669-692. doi: 10.5636/jgg.46.669

Nozdrachev, M. N., Skalsky, A. A., Styazhkin, V. A., & Petrov, V. G. (1998, May).

Some Results of Magnetic Field Measurements by the FM-3I Flux-Gate Instrument Onboard the INTERBALL-1 Spacecraft. *Cosmic Research*, *36*(3), 251.

Petrukovich, A. A., Chugunova, O. M., & Shustov, P. I. (2019, September). Low-frequency magnetic variations at the high-β Earth bow shock. *Annales Geophysicae*, *37*(5), 877-889. doi: 10.5194/angeo-37-877-2019

Plaschke, F., Hietala, H., Archer, M., Blanco-Cano, X., Kajdič, P., Karlsson, T., ... Sibeck, D. (2018, August). Jets Downstream of Collisionless Shocks. *Space Science Reviews*, *214*(5), 81. doi: 10.1007/s11214-018-0516-3

Pokhotelov, O. A., & Balikhin, M. A. (2012, July). Weibel instability in a plasma with nonzero external magnetic field. *Annales Geophysicae*, *30*, 1051-1054. doi: 10.5194/angeo-30-1051-2012

Pollock, C., Moore, T., Jacques, A., Burch, J., Gliese, U., Saito, Y., ... Zeuch, M. (2016, March). Fast Plasma Investigation for Magnetospheric Multiscale. *Space Science Reviews*, *199*(1-4), 331-406. doi: 10.1007/s11214-016-0245-4

Rème, H., Aoustin, C., Bosqued, J. M., Dandouras, I., Lavraud, B., Sauvaud, J. A., ... Sonnerup, B. (2001, October). First multispacecraft ion measurements in and near the Earth's magnetosphere with the identical Cluster ion spectrometry (CIS) experiment. *Annales Geophysicae*, *19*, 1303-1354. doi: 10.5194/angeo-19-1303-2001

Russell, C. T., Anderson, B. J., Baumjohann, W., Bromund, K. R., Dearborn, D., Fischer, D., ... Richter, I. (2016, March). The Magnetospheric Multiscale Magnetometers. *Space Science Reviews*, *199*(1-4), 189-256. doi: 10.1007/s11214-014-0057-3

Sagdeev, R. Z. (1966, January). Cooperative Phenomena and Shock Waves in Collisionless Plasmas. *Reviews of Plasma Physics*, *4*, 23.

Scudder, J. D., Mangeney, A., Lacombe, C., Harvey, C. C., Aggson, T. L., Anderson, R. R., ... Russell, C. T. (1986, October). The resolved layer of a collisionless, high β, supercritical, quasi-perpendicular shock wave 1. Rankine- Hugoniot geometry, currents, and stationarity. *Journal of Geophysical Research*, *91*, 11019-11052. doi: 10.1029/JA091iA10p11019

Turner, D. L., Wilson, L. B., Liu, T. Z., Cohen, I. J., Schwartz, S. J., Osmane, A., ... Burch, J. L. (2018, September). Autogenous and efficient acceleration of energetic ions upstream of Earth's bow shock. *Nature*, *561*(7722), 206-210. doi: 10.1038/s41586-018-0472-9

Urbář, J., Němeček, Z., Å afránková, J., & Přech, L. (2019, August). Solar Wind Proton Deceleration in Front of the Terrestrial Bow Shock. *Journal of Geophysical Research (Space Physics)*, *124*(8), 6553-6565. doi: 10.1029/2019JA026734

Winterhalter, D., & Kivelson, M. G. (1988, September). Observations of the Earth's bow shock under high Mach number/high plasma beta solar wind conditions. *Geophysical Research Letters*, *15*, 1161-1164. doi: 10.1029/GL015i010p01161